

ELLIPTIC FLOW FROM AN ON-SHELL PARTON CASCADE

D. MOLNÁR and M. GYULASSY

Physics Department, Columbia University

538 West 120th Street, New York, NY 10027, U.S.A.

E-mail: molnard@phys.columbia.edu, gyulassy@nt3.phys.columbia.edu

Differential elliptic flow out to $p_{\perp} \sim 5$ GeV/c is calculated using the MPC elastic parton cascade model^{1,2} for Au+Au at $E_{cm} \sim 130$ A GeV. The results are compared to recent STAR/RHIC elliptic flow data³. An elliptic flow pattern comparable to the data seems to require initial parton densities at least twice higher than the predicted by the HIJING model⁴. Elliptic flow is also shown to be sensitive to the hadronization procedure.

1 Introduction

Elliptic flow, $v_2(p_{\perp}) = \langle \cos(2\phi) \rangle_{p_{\perp}}$, the differential second moment of the azimuthal momentum distribution, has been the subject of increasing interest^{5,6,7,8,9} since the discovery³ at RHIC that $v_2(p_{\perp} > 1 \text{ GeV}) \rightarrow 0.2$. This sizable high p_{\perp} collective effect depends strongly on the dynamics in a heavy ion collision and provides important information about the density and effective energy loss of partons.

The simplest theoretical framework to study elliptic flow is ideal hydrodynamics⁵. For RHIC energies, ideal hydrodynamics agrees remarkably well with the measured elliptic flow data³ up to transverse momenta ~ 1.5 GeV/c. However, it fails to saturate at high $p_{\perp} > 2$ GeV as does the data reported by STAR at Quark Matter 2001.

A theoretical problem with ideal hydrodynamics is that it assumes local equilibrium throughout the whole evolution. This idealization is marginal for conditions encountered in heavy ion collisions². A theoretical framework is required that allows for nonequilibrium dynamics. Covariant Boltzmann transport theory provides a convenient framework that depends on the local mean free path $\lambda(x) \equiv 1/\sigma n(x)$. It interpolates between free streaming ($\lambda = \infty$) and ideal hydrodynamics ($\lambda = 0$).

Parton cascade simulations^{6,7,10} show on the other hand, that the initial parton density based on HIJING⁴ is too low to produce the observed elliptic flow unless the pQCD cross sections are artificially enhanced by a factor $\sim 2 - 3$. However, gluon saturation models¹¹ predict up to five times higher initial densities, and these may be dense enough to generate the observed collective flow even with pQCD elastic cross sections. In this study, we explore

the dependence of elliptic flow on the initial density, or equivalently^a, on the partonic cross section.

Calculations based on inelastic parton energy loss^{8,9} also predict saturation or decreasing v_2 at high p_\perp . These calculations are only valid for high p_\perp , where collective transverse flow from lower p_\perp partons can be neglected. The hydrodynamic component from low p_\perp is, on the other hand, automatically incorporated in parton cascades. Though parton cascades lack at present covariant inelastic energy loss, we find in Fig. 1 that elastic energy loss alone may account for the observed high p_\perp azimuthal flow pattern as long as the elastic opacity is large enough.

We compute the partonic evolution with MPC¹, a newly formulated, covariant, parton kinetic theory technique. MPC is an extension of the covariant parton cascade algorithm, ZPC¹². Both MPC and ZPC have been extensively tested^{13,14} and compared to analytic transport solutions and covariant Euler and Navier-Stokes dynamics in 1+1D geometry. A critical new element of both these algorithms is the parton subdivision technique proposed by Pang^{14,15}.

2 Covariant Parton Transport Theory

We consider here, as in Refs.^{1,2,12,15}, the simplest form of Lorentz-covariant Boltzmann transport theory in which the on-shell phase space density $f(x, \mathbf{p})$, evolves with an elastic $2 \rightarrow 2$ rate as

$$p_1^\mu \partial_\mu f_1 = \iiint_{234} (f_3 f_4 - f_1 f_2) W_{12 \rightarrow 34} \delta^4(p_1 + p_2 - p_3 - p_4) + S(x, \mathbf{p}_1). \quad (1)$$

Here W is the square of the scattering matrix element, the integrals are short-hands for $\int \equiv \int \frac{g}{(2\pi)^3 E_i} \frac{d^3 p_i}{i}$, where g is the number of internal degrees of freedom, while $f_j \equiv f(x, \mathbf{p}_j)$, and we interpret $f(x, \mathbf{p})$ as describing an ultrarelativistic massless gluon gas with $g = 16$ (8 colors, 2 helicities). The initial conditions are specified by the source function $S(x, \mathbf{p})$, which we discuss in Section 4.

The elastic gluon scattering matrix elements in dense parton systems are modeled by a Debye-screened form

$$\frac{d\sigma}{dt} = \sigma_0 \left(1 + \frac{\mu^2}{s} \right) \frac{\mu^2}{(t - \mu^2)^2}, \quad (2)$$

where μ is the screening mass, $\sigma_0 = 9\pi\alpha_s^2/2\mu^2$ is the total cross section, which we chose to be independent of energy. For a fixed σ_0 , the relevant transport cross section $\sigma_t = \int d\sigma \sin^2 \theta_{cm}$ is maximal in the isotropic ($\mu \rightarrow \infty$) case.

^a The equivalence is due to the scaling property explained in Section 3.

It is important to emphasize that while the cross section suggests a geometrical picture of action over finite distances, Eq. (2) is only a convenient parametrization to describe the effective *local* transition probability, W , as $dW/dt = s d\sigma/dt$. The particle subdivision technique (see next Section) removes all notion of nonlocality in this approach, as in hydrodynamics.

3 Parton Subdivision and Scaling of Solutions

Cascade algorithms inevitably violate Lorentz covariance because particle interactions are assumed to occur whenever the distance of closest approach (in the relative c.m.) is $d < \sqrt{\sigma_0/\pi}$, which corresponds to action at a distance. To recover the *local* character of equation (1) and hence Lorentz covariance, we use the parton subdivision technique^{12,15}. This technique is based on the covariance of Eq. (1) under the transformation

$$f \rightarrow f' \equiv l f, \quad W \rightarrow W' \equiv W/l \quad (\sigma \rightarrow \sigma' = \sigma/l), \quad (3)$$

which effectively rescales the cascade interaction range by $1/\sqrt{l}$. Lorentz violation formally vanishes¹⁴ in the $l \rightarrow \infty$ limit. In practice, very high $\sim 100 - 1000$ subdivisions are needed² to obtain accurate numerical solutions from initial conditions expected at RHIC.

Subdivision covariance (3) implies that the transport equation has a broad dynamical range, and the solution for any given initial condition and transport property immediately provides the solution to a broad band of suitably scaled initial conditions and transport properties. This is because solutions for problems with l times the initial density $dN/d\eta$, but with one l -th the reaction rate can be mapped to the original ($l = 1$) case. We must use subdivision to eliminate numerical artifacts. However, once that is achieved, we have actually found the solution to a whole class of suitably rescaled problems.

The dynamical range of Eq. (1) is further increased by its covariance under coordinate and momentum rescaling², leading to covariance under

$$f(x, \vec{p}) \rightarrow f'(x, \vec{p}) \equiv l_p^{-3} l f\left(\frac{x}{l_x}, \frac{\vec{p}}{l_p}\right),$$

$$W(\{p_i\}) \rightarrow W'(\{p_i\}) \equiv \frac{l_p^2}{l_x l} W\left(\left\{\frac{p_i}{l_p}\right\}\right), \quad m \rightarrow m' = m/l_p, \quad (4)$$

where l_x and l_p are the coordinate and momentum scaling parameters, respectively. This means² that we can scale one solution to others provided that μ/T_0 , $\sigma_0 dN/d\eta$ and R_0/τ_0 remain the same.

4 Results and Discussion

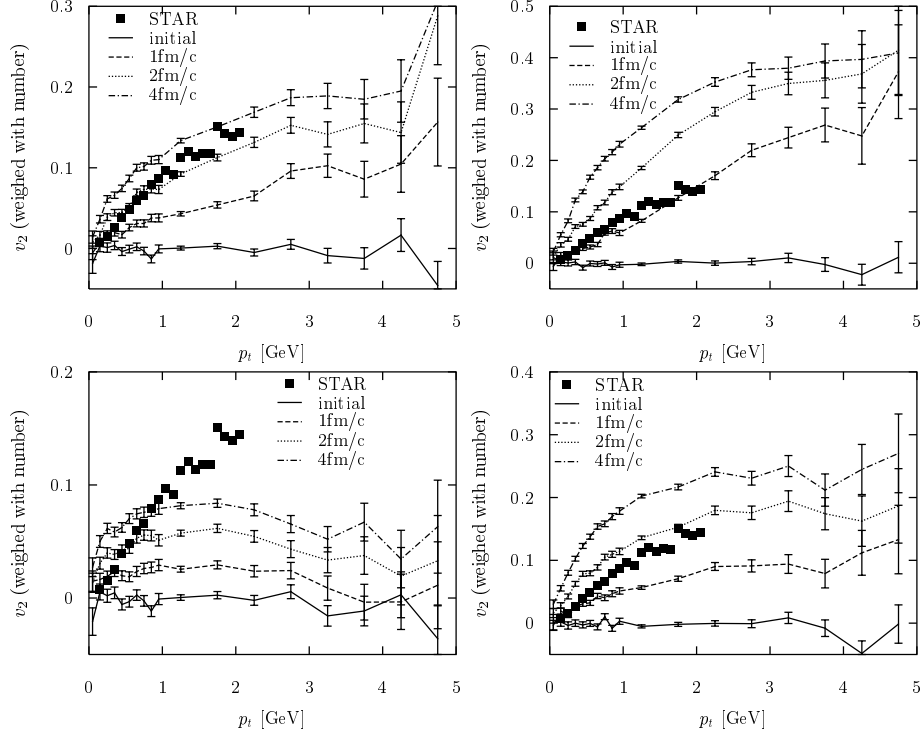


Figure 1. The proper time evolution of elliptic flow as a function of transverse momentum, for an Au+Au collision at $\sqrt{s} = 130A$ GeV with $b = 8$ fm, in case of isotropic (top row) and gluonic (bottom row) cross section with $\sigma_0 = 3$ mb (left) and 10 mb (right).

Following Ref.⁶, we modeled the colliding nuclei as longitudinally boost invariant Bjorken cylinders with radii $R_0 = 6$ fm in local thermal equilibrium at temperature T_0 at proper time $\tau_0 = 0.1$ fm/c. The pseudo-rapidity $\eta \equiv 1/2 \log((t+z)/(t-z))$ distribution was taken as uniform between $|\eta| < 5$. For central collisions, $T_0 = 500$ MeV and $dN/d\eta = 400$ as by fitting the gluon mini-jet transverse momentum spectrum predicted by HIJING⁴ (including shadowing and jet quenching effects). For non-central collisions, as a crude estimate, we scaled $dN/d\eta$ by the overlap area of the two cylinders. To maximize elliptic flow, the impact parameter was chosen to be $b = 8$ fm.

Evolutions from different initial densities can be obtained by varying the cross section only and using the scaling property explained in Section 3. Our simulations were performed both with isotropic and gluonic cross sections

($\mu = 0.5$ GeV) with $\sigma_0 = 3$ and 10 mb. The particle subdivision was $l = 100$.

Fig. 1 shows the proper time evolution of the gluon elliptic flow as a function of transverse momentum for the different cross sections. For all cross sections studied, elliptic flow reaches its final asymptotic value early, by $\tau = 4$ fm/ c , reinforcing results in Ref. ⁶. Also, elliptic flow increases with increasing *transport* cross section, as expected.

Elliptic flow monotonically increases until $p_{\perp} \sim 2$ GeV, where it saturates. According to a more detailed study¹⁰, this saturation occurs for all impact parameters, leading to a saturation in the impact parameter averaged (minimum bias) elliptic flow as well. For the 3 mb gluonic cross section, v_2 decreases after 2 GeV, due to elastic energy loss.

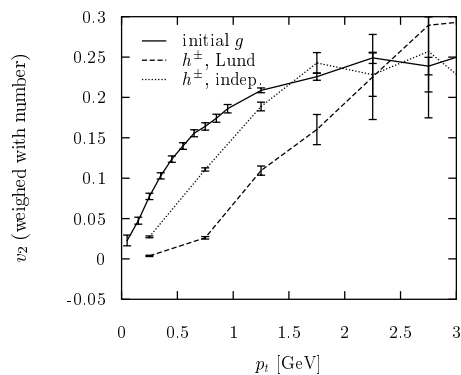


Figure 2. Partonic and the final hadronic elliptic flow after hadronization via independent or Lund fragmentation, for the 10 mb gluonic cross section.

Fig. 2 shows the effect of hadronization on elliptic flow. Two extreme cases are presented: independent fragmentation and Lund fragmentation via 400 long ($\Delta y = 10$) strings. In the case of independent fragmentation, the produced hadrons move in slightly different direction than the original parton (jet cone effect), resulting in a moderate reduction of elliptic flow. Lund fragmentation produces all hadrons with almost complete azimuthal symmetry^b, leading to an order of magnitude reduction at low p_{\perp} .

5 Conclusion

The elliptic flow results from the parton cascade MPC^{1,2} strongly suggest that the observed saturation of elliptic flow at $p_{\perp} \sim 2$ GeV can be *quantitatively*

^b The azimuthal symmetry is not perfect because the gluons kink the strings, however, the kinks are very small.

reproduced from parton kinetic theory, if the initial parton density is high enough. In addition, the sensitivity of elliptic flow on hadronization scheme will provide a strong constraint on possible hadronization scenarios. A more detailed study of these issues is in progress¹⁰.

Acknowledgments

We acknowledge the Parallel Distributed Systems Facility at the National Energy Research Scientific Computing Center for providing computing resources.

This work was supported by the Director, Office of Energy Research, Division of Nuclear Physics of the Office of High Energy and Nuclear Physics of the U.S. Department of Energy under contract No. DE-FG-02-93ER-40764.

References

1. D. Molnár, MPC 1.0.9. Parton cascade code used in present study can be downloaded at <http://nt3.phys.columbia.edu/people/molnard>.
2. D. Molnar and M. Gyulassy, Phys. Rev. **C 62**, 054907 (2000).
3. K. H. Ackermann *et al.*, Phys. Rev. Lett. **86**, 402 (2001).
4. M. Gyulassy and X. Wang, Comput. Phys. Commun. **83**, (1994) 307.
5. J. Ollitrault, Phys. Rev. **D 46**, 229 (1992); P. F. Kolb, P. Huovinen, U. Heinz and H. Heiselberg, hep-ph/0012137.
6. B. Zhang, M. Gyulassy and C. M. Ko, Phys. Lett. **B455**, 45 (1999).
7. S. A. Bass *et al.*, Nucl. Phys. **A661**, 205 (1999) [nucl-th/9907090].
8. X. Wang, nucl-th/0009019.
9. M. Gyulassy, I. Vitev and X. N. Wang, nucl-th/0012092.
10. D. Molnár and M. Gyulassy, “Elliptic flow and particle spectra from the parton cascade MPC”, *in preparation*
11. K. J. Eskola, K. Kajantie, P. V. Ruuskanen, and K. Tuominen, Nucl. Phys. **B570**, 379 (2000) [hep-ph/9909456].
12. B. Zhang, Comput. Phys. Commun. **109**, 193 (1998) [nucl-th/9709009].
13. M. Gyulassy, Y. Pang, and B. Zhang, Nucl. Phys. **A626**, (1997) 999.
14. B. Zhang, M. Gyulassy, and Y. Pang, Phys. Rev. C **58**, (1998) 1175.
15. Y. Pang, RHIC 96 Summer Study, CU-TP-815 preprint (unpublished); Generic Cascade Program (GCP) documentation available at WWW site <http://rhic.phys.columbia.edu/rhic/gcp>.
16. *Proc. of Open Standards for Cascade Models for RHIC (OSCAR)*, BNL-64912, June 23-27, 1997, eds. M. Gyulassy and Y. Pang; Source codes and documentation for transport models under the OSCAR standard can be downloaded at <http://nt3.phys.columbia.edu/OSCAR/>